Single-Walled Carbon Nanotubes in Nanosized Basalts as Nanocomposites: The Electrical/Dielectric Properties and Electromagnetic Interference Shielding Performance

Reem Alwafi[1] · Abdu Saeed[1,2,3]

Abstract

About 90 of the volcanic rocks worldwide are basalt rocks utilized to produce basalt fibers. They are considered insulators electrically. Herein, the basalts' electrical/dielectric properties have been significantly enhanced by introducing single-walled carbon nanotubes (SWCNT) to the basalt nanosized. We obtained nanosized basalt powders using ball milling with an average particle size of 67.86 nm. The basalt nano-powders were suspended on ethanol and mixed with SWCNT under rigorous sonication and stirring. Basalt/SWCNT nanocomposites were produced with SWCNT ratios 0, 1, 3, and 5 wt%. We evaluated their electrical conductivity, dielectric constant, and dielectric loss at different frequencies and temperatures ranging from room temperature (RT) to 1200 Kelvin. The results at 20 kHz revealed that the pure basalts' electrical conductivity was 1.16×10^{-7} S/cm at RT. At the same time, it was 0.03, 0.19, and 0.46 S/cm for the basalt/SWCNT nanocomposites at the SWCNT ratios 1, 3, and 5 wt%, respectively. These results proved that the basalts turned from insulators to become conductors even at the lowest ratio of SWCNT, i.e., 1 wt%. The basalt/SWCNT nanocomposites' dielectric constant increased thousands of folds compared with pure basalts. Besides, theoretical calculations demonstrated a superior electromagnetic interference shielding (EMI) performance for the prepared nanocomposites. This study's findings could open new horizons for using SWCNT in basalt for EMI shielding applications.

✉ Abdu Saeed
Abdusaeed79@hotmail.com; Abdusaeed@tu.edu.ye

1   Department of Physics, Faculty of Science, King Abdulaziz University, Jeddah 21589, Saudi Arabia

2   Center of Nanotechnology, King Abdulaziz University, Jeddah 21589, Saudi Arabia

3   Department of Physics, Thamar University, 87246 Thamar, Yemen

Graphical Abstract

Basalt/SWCNT nanocomposites were prepared and showed dramatically enhanced electrical conductivity, dielectric constant, and good EMI shielding performance.
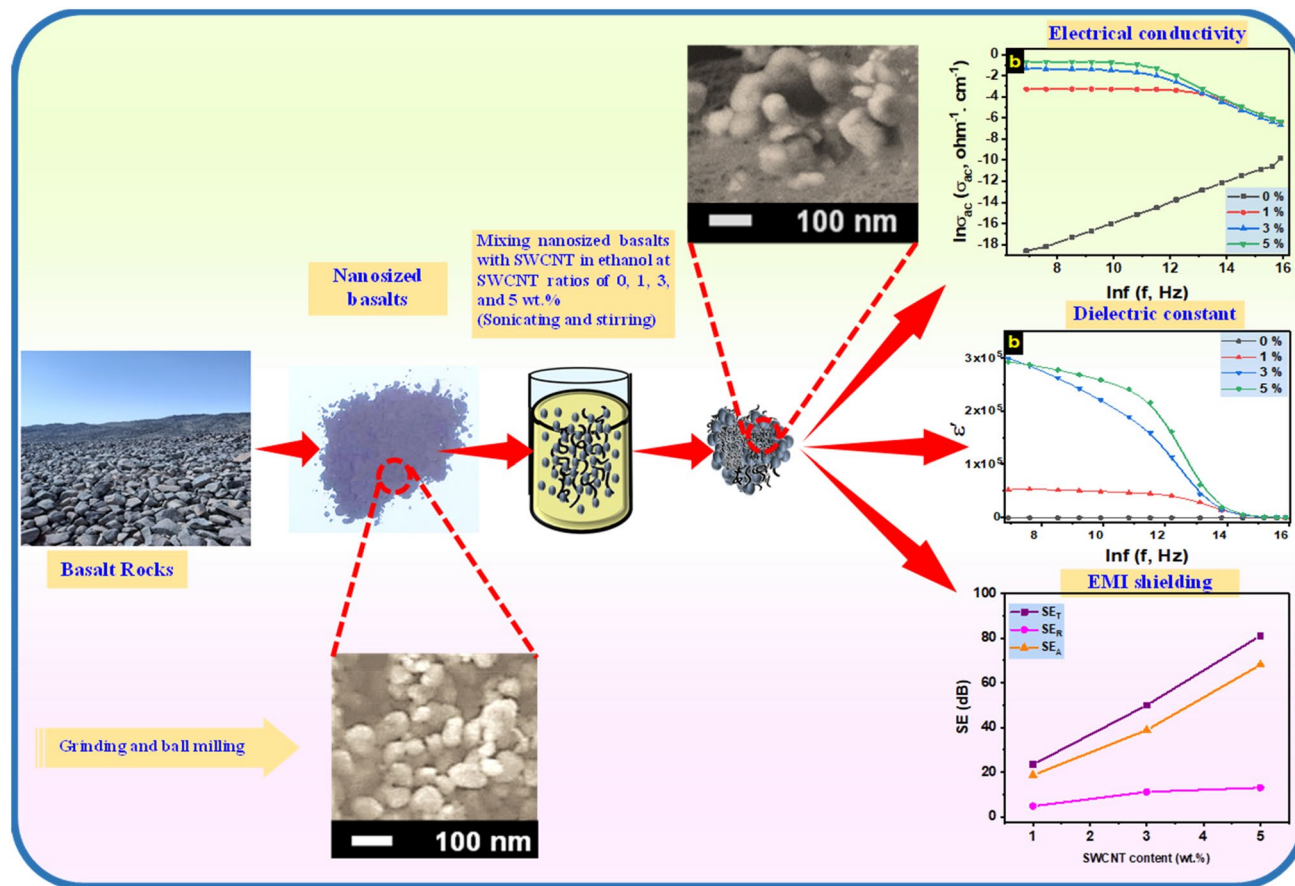
Keywords Nano basalt · SWCNT · Nanocomposite · Electrical conductivity · Dielectric constant · Dielectric loss · EMI shielding

1 Introduction

Basalts are the most widespread volcanic rocks; they are mafic extrusive igneous rocks formed during lava's rapid cooling. Although they include different elements such as calcium (Ca), potassium (K), phosphorus (P), sulfur (S), silicon (Si), and sodium (Na) [1–3]; they also are rich in magnesium (Mg) and iron (Fe) [3, 4]. Depending on their chemical elemental composition, they have a spectrum of colors; they can be dark, brown, gray, and pale green [5]. Around 70% of the Earth's surface areas are covered by basalts rocks [6], which make up large areas of lava in different places in the world, for instance, the Deccan Plateau, Hawaii, Iceland, India, and the majority of the seafloor [7]. The widespread abundance of basalt makes them cheap raw material to produce glass and ceramics using different thermal treatment methods [8]. Besides, they are used in construction as building materials, blocks, and highway engineering. The beauty of using basalts for many applications is that they are environmentally natural raw materials; they do not produce any toxic when are used as raw materials in the industry.

Although different materials' fibers are applied in many applications, the basalt fibers, glass fibers, and carbon fibers are most important due to their gigantic prominence in the economy of industrial nations. For instance, fiber composites materials have been growing and contributing to the China economy, with an average annual growth of more than thirty percent [9]. Given this point, basalt rocks are the raw materials for manufacturing basalt fibers, which have high stiffness and strength, reasonable cost, excellent oxidation/corrosion resistance, and thermal

stability [10]. They take possession of better mechanical properties than glass fibers and are considerably cheaper than carbon fibers [11]. Therefore, they have been used to reinforce and enhance the properties of the geopolymer and polymer in so-called basalt fiber-reinforced polymers (BFRPs) [1, 12–15]. Besides, basalt fibers can be used for radiation shielding [4]. They are vastly utilized for both civilian and military applications. In civilian applications, they are used in medicine and chemical industries, agriculture, architecture, aerospace, and electronics; they can be described as novel materials in the twenty-first century [9, 16].

Carbon nanotubes (CNT) are utilized, as high-conductivity material with unique properties, to produce nanocomposites. Nanocomposites Based on CNT, polyvinylidene, and magnetite were prepared for energy dissipation of electromagnetic waves [17]. Single-walled carbon nanotube (SWCNT) as CNT has been used to enhance the electrical properties of different polymers in the form of polymer/SWCNT composites such as poly(ether ether ketone) (PEEK)/SWCNT composites [18], flexible poly(3,4 ethylene dioxythiophene)-tosylate/SWCNT composites [19], carbon fiber-reinforced polymers (CFRP)/SWCNT composites [20], and polyvinylidene fluoride (PVDF)/SWCNT composites [21]. Although the SWCNT was used with rocks to form aluminosilicate/SWCNT composites [22], SWCNT was used to incorporate rocks rarely. Many scientific reports investigated the basalts and their fibers' electrical conductivity and dielectric properties [1, 10, 23]. They found that the basalts showed low electrical conductivity. Besides, studies aimed to enhance the basalts' electrical and dielectric properties by fabricating them with conductor polymers [1, 23]. Although the CNTs have been used recently [10] to grow on basalt fibers for electromagnetic interference shielding (EMI) purposes; however, to the best of our knowledge, the electrical and dielectric properties of basalts/ SWCNT composites have not been investigated yet. Therefore, we aimed in this study to promote the electrical and dielectric properties of basalt through the fabrication of nanosized basalts/ SWCNT composites. The basalt rocks were turned into nanosized powders via the physical ball milling technique; they were mixed with SWCNT ratios of 0, 1, 3, and 5 wt%. The elemental compositions and structural properties of the fabricated nanosized basalts/SWCNT composites were then explored. The electrical and dielectric properties of the fabricated composites were investigated in the wide temperature range of 300–1200 Kelvin at different applied electrical frequencies starting from 1 kHz up to 8 MHz. Besides, the EMI shielding performances of the prepared nanocomposites were estimated. More details of the methodology and the obtained results were included in the following sections.

2 Materials and Methods

2.1 Samples' Collection and Preparation of Nanosized Basalts

The basalt rocks were collected from the western region of Saudi Arabia, which is rich in volcanic rocks. They were collected precisely from Harrat al Muhaysiniyah and Harrat al Thaniyah near Jeddah city (Fig. S1). The collected basalts were utilized to prepare nanosized basalts/SWCNT composites, as illustrated in Fig. S2. Briefly, the collected basalts rocks were ground until they became powders in microsized as described in the published work [24] with some modifications. The basalts were ground as a first stage using the CRUSHER BB 300 model (Retsch-Allee Haan, Germany); then, they were ground as a second stage via a ROLL CRUSHER model (Sew-Eurodrive GmbH & Co KG, Germany). After that, they were ground as a third stage using a laboratory ROLLER MILL model (Sew-Eurodrive GmbH & Co KG, Germany). These three phases produced microsized powders of basalts. Then, the chemical elemental compositions of the microsized powders were investigated via the energy-dispersive X-ray spectroscopy (EDS) JSM-7600F model (JEOL, Japan). Besides, by the EDS mapping technique, mapping was performed for the highest four elements in the basalts' powders to show their distribution. The nanosized basalts were prepared by ball milling the microsized basalt powders at room temperature (RT) in a rolling ball mill with high energy via the PM 400 model (Retsch-Allee Haan, Germany). A10 g of the microsized basalt powders were added into the milling jar (250 ml); we used steel balls to perform the milling operation. The sample to ball mass ratio was set at 1:16. The milling procedure persisted for 50 h (2 min rotation/2 min stopping) with a rotation speed of 200 rpm.

2.2 Composites Fabrications

The obtained nanosized basalts were mixed with SWCNT (Adnano Technologies, India); the average diameters of SWCNT are about ~ 1.4 nm with a length ~ of 400 nm −> 2 μm according to the datasheet from the manufacturer. The basalts/SWCNT composites were prepared at SWCNT ratios of 0, 1, 3, and 5 wt%. The mixtures of nanosized basalts/SWCNT (1 g) were suspended in ethanol (200 mL). To get homogenous mixtures, first, the nanosized basalts/ SWCNT mixtures in ethanol were subjected for 5 min to high power probe sonicator, model UIP500hdT (Hielscher, USA). Then, they were again subjected to sonication and stirring; the sonication was performed this time using an ultrasonic bath, model CPX 5800 (Branson Ultrasonics,

USA); the sonication and stirring were alternated for 1 h for each, a total time of 4 h. After that, they were dried at 70 ºC in the oven. Finally, the dried nanosized basalt/SWCNT composites were collected, characterized, and prepared for electrical/dielectric measurements. Fig. S3 shows the nanosized basalts powder, SWCNT, and the prepared basalts/SWCNT nanocomposite at the SWCNT ratio of 5 wt%.

2.3 Characterization Techniques

The nanosized basalt/SWCNT composites were imaged via scanning electron microscope (SEM) JSM-7600F model (JEOL, Japan) to investigate their morphology and SWCNT distribution. The X-ray diffraction (XRD) patterns were recorded with the same parameters reported in the published work [25] via the X-ray diffractometer Ultima IV model (Rigaku, Japan) to estimate the crystalline phases of the composites. The XRD patterns were indexed and matched according to the International Centre for Diffraction Data (ICDD) cards. The nanosized basalt/SWCNT composites' molecular structures were studied using the Raman spectroscopy DXR model (Thermo Scientific, USA), equipped with a 532 nm diode-pumped solid-state laser. The Raman spectra were recorded at 5 mW excitation laser power, with collection time exposure of 2 s, and accumulation exposure number of 40. Besides, Fourier-transform infrared spectroscopy (FTIR) Nicolet iS10 FTIR model (Thermo Scientific, USA) was also used to investigate the chemical functional groups of the fabricated composites in the FTIR spectral range of 4000–600 cm^{-1} with the attenuated total reflection (ATR) sampling technique. Thermogravimetric analysis (TGA) and differential scanning calorimetry (DSC) were used to explore the thermal stability of the prepared basalts/SWCNT nanocomposites in the temperature range of 300–1200 Kelvin with a heating rate of 10 °C/min at air atmosphere using NETZSCH model STA 449 F3 Jupiter (NETZSCH-Gerätebau GmbH, Germany).

2.4 Electrical and Dielectric Measurements

For electrical/dielectric properties measurements, the prepared nanosized basalts/SWCNT composites were investigated and scanned via an impedance analyzer LCR bridge using the Hioki LCR METER IM3536 model (Hioki, Japan). The powders of the prepared nanosized basalts/SWCNT composites were pressed in a die to form pellets, as stated by the published studies [26–31]. Briefly, they were pressed in a die with a diameter of 13 mm to make up pellets with an average thickness of 2 mm. Polyvinyl alcohol (PVA) (Sigma-Aldrich-USA) was used as a binder with a weight ratio of 3 wt%. The pellets were heated at 250 °C for 3 h to evaporate the PVA. Then, the flat pellets' faces were polished and coated by thin layers of conductive high-performance silver paste (Ted Pella Inc, USA) to form the electrodes of the pellets. Then, the electrical and dielectric measurements were performed at temperature and frequency ranges of 300–1200 K and 1 kHz–8 MHz, respectively. The electrical and dielectric measurements were performed under the air atmosphere. The alternating current (ac) electrical conductivity (σ_{ac}) was estimated through the following equation [32–34]:

$$\sigma_{ac} = G_p \frac{t}{A} \tag{1}$$

where G_p is the measured parallel conductance of the pellet. The t and A are the thickness and face area of the measured sample (pellet), respectively.

To investigate the dielectric properties, the real part (ε') and the imaginary part (ε'') of the permittivity (ε^*) were estimated. Where ε^* is a complex quantity that is given by [32, 33]:

$$\varepsilon^* = \varepsilon' - j\varepsilon'' \tag{2}$$

The ε' symbolizes the dielectric constant, while the ε'' represents the dielectric loss of the sample. Equations 3 and 4 were used to estimate ε' and ε'', respectively [30, 32]:

$$\varepsilon' = \frac{C_p t}{\varepsilon_o A} \tag{3}$$

$$\varepsilon'' = \varepsilon' \tan\delta \tag{4}$$

C_p symbolizes the measured parallel capacitance of the pellet; ε_o and $\tan\delta$ symbolize the permittivity of free space and the measured tangent loss, respectively.

2.5 EMI Shielding Calculations

The EMI shielding ability of the prepared basalt/SWCNT nanocomposites at the X-band (8.2–12.4 GHz) was estimated theoretical using Simon's formula [35]:

$$SE_T = 50 + 10\log\left(\frac{\sigma}{f}\right) + 1.7d(f\sigma)^{1/2} \tag{5}$$

where SE_T is the total shielding efficiency, σ is the measured electrical conductivity in S/cm, f is the frequency in MHz, and d is the sample thickness in cm, which is greater than the skin depth. Then, the absorption shielding efficiency (SE_A) and the reflection shielding efficiency (SE_R) can also be calculated using the following expressions [35, 36]:

$$SE_A = 1.7d(f\sigma)^{1/2} \tag{6}$$

$$SE_R = 50 + 10\log\left(\frac{\sigma}{f}\right) \tag{7}$$

3 Results and Discussion

3.1 Structural Properties

We studied the powders of the raw basalts by EDS to estimate the basalts' quantitively and qualitative chemical elements. Figure 1 exhibits the obtained EDS results; Fig. 1a displays the SEM image of the basalts; it indicates an area of 25×25 µm used for every EDS analysis; we used five different sites to perform EDS analysis. While Fig. 1b shows the obtained EDS spectrum, which points out that the basalt samples contain O, Na, Mg, Al, Si, Ca, Ti, and Fe elements. Figure 1c exhibits the weight ratio of these elements; the pie chart demonstrates the weight ratio; it shows that the weight ratios of O, Na, Mg, Al, Si, Ca, Ti, and Fe elements are 45.26, 1.72, 4.34, 6.59, 21.02, 6.28, 0.94, and 13.85%, respectively. The four elements with the highest ratio are O, Si, Fe, and Al, whose EDS-mapping are shown in Figs. 1d–g; the figures of the EDS mapping show the distribution of O (green), Si (white), Fe(red), and Al (yellow). Figure 1h displays the EDS mapping for the overlap of the mixed four elements. Table 1 lists the atomic percent ratio of the chemical elements in the tested basalts.

Figure 2 shows SEM images of the prepared nanosized basalts/SWCNT composites' powders. The SEM image

in Fig. 2a belongs to the powder of nanosized basalts at the magnification of $\times 20{,}000$. For estimating the particle size of the nanosized basalts, an image of SEM was taken at the magnification of 40,000 X and shown in Fig. 2b. Simultaneously, the histogram particle size distributions of the nanosized basalts were made from the SEM image at the magnification of 40,000 X and shown in Fig. 2c. The average particle size is 67.86 ± 31.94 nm. The broad particle size distributions could be illustrated being the basalts comprising different minerals with different mechanical properties such as texture and hardness that impact the milling operation and subsequently produce particles of different sizes [30]. The SEM images in Figs. 2e, d belong to prepared nanosized basalts/SWCNT composites' powders at SWCNT ratios 1, 3, and 5 wt%, respectively. As expected, the SEM images in Figs. 2d–f clearly explain the increasing SWCNT distribution by increasing its ratio from 1 wt% to 5 wt%. Besides, the SWCNT appears as bundles or nets reflecting its aggregation in the SWCNT. Furthermore, Figs. 2d–f show that the basalt"particles' surfaces seemed with lobed surface and seem larger than those in the pure basalt powders. The basalt particles' size distribution (Fig. 2c) could explain this notice; it recorded sizes up to 160 nm (mean size was 67.86 ± 31.94 nm). Therefore, the smaller basalts particles could enter the SWCNT bundles and nets under rigorous stirring and sonication for 4 h. In contrast, the larger basalts particles
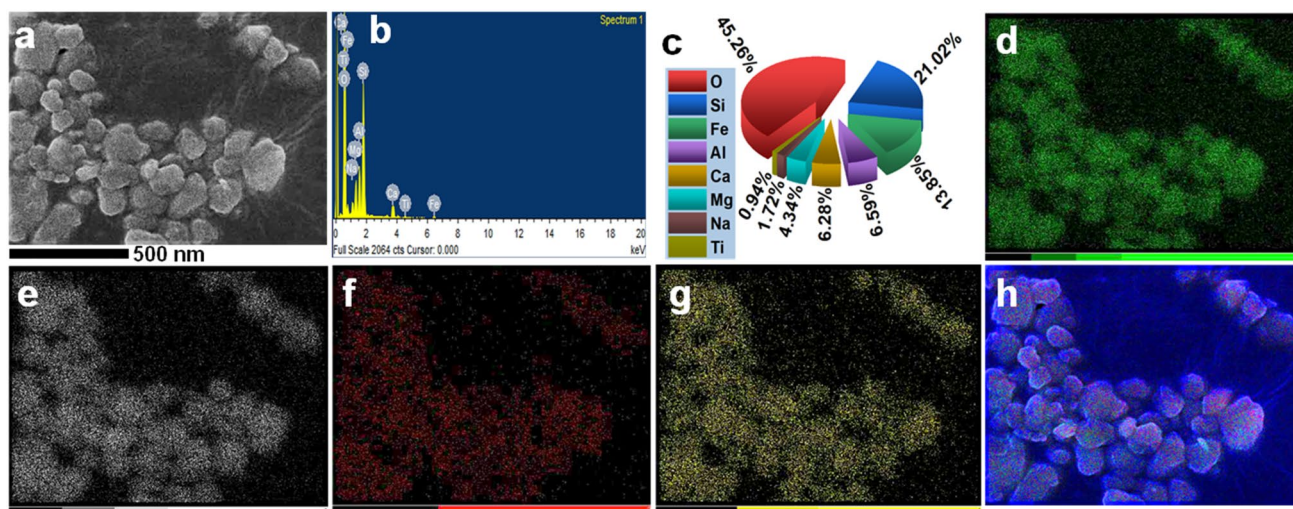

Fig. 1 SEM–EDS of the basalt (**a**) SEM image, (**b**) EDS spectrum, (**c**) the weight ratio of the chemical elemental composition represented by the pie chart, (**d**-**g**) EDS-mapping images for the individual element distribution of O (green), Si (white), Fe (red), and Al (yellow), respectively, and (**h**) EDS-mapping for the mixed distributions of O, Si, Fe, and Al (Color figure online)

Table 1 Atomic percent ratio of the chemical elements in the basalt via obtained via EDS

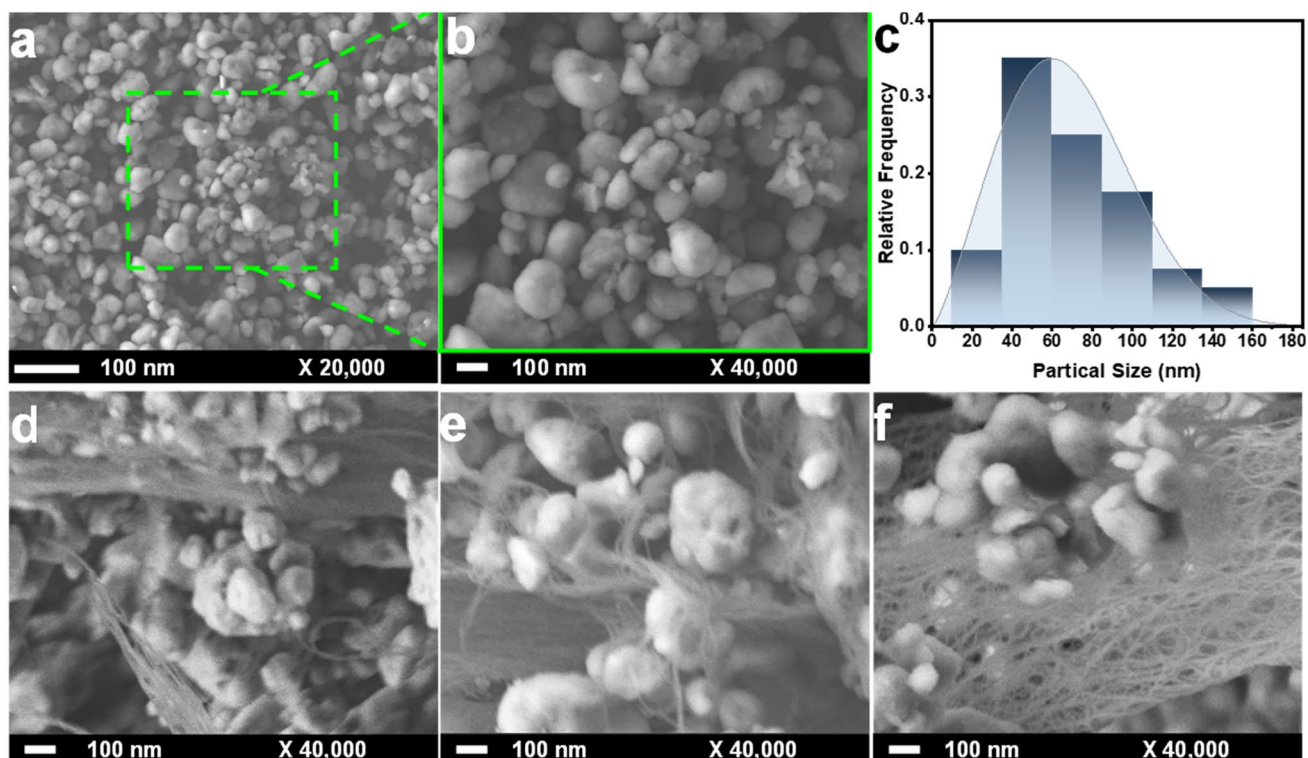| Element	O	Na	Mg	Al	Si	Ca	Ti	Fe
Atomic%	62.48	1.67	3.97	5.43	16.63	3.48	0.44	5.51

Fig. 2 **a** and **b** SEM images of the pure nanosized basalts at the magnification of 20,000 and 40,000 X, respectively **c** histogram particle size distributions of the nanosized basalts' powder. Nanosized basalts/SWCNT composites' powders at SWCNT ratios of (**d**) 1, (**e**) 3, and (**f**) 5 wt%

stay on the surfaces of the SWCNT bundles and nets. Also, the lobed surfaces might indicate aggregating in the basalt particles while drying the nanosized basalts/SWCNT composites.

We used XRD to investigate the crystallinity and define the crystal phases included in the pure basalts and crystallinity changes in the prepared nanosized basalts/SWCNT

composites' powders at SWCNT ratios 0, 1, 3, and 5 wt%. The obtained XRD patterns are shown in Fig. 3a. The B-spline function was used to fit the XRD patterns' shapes. The XRD of the pure basalt (0 wt% of SWCNT ratio) showed different diffraction peaks at 2θ values of 28.47, 31.53, 32.11, 35.68, 43.42, 48.38, 63.99, 73.14, 75.65, and 77.14°. The quantitative XRD phase analysis was implemented in

Fig. 3 XRD of nanosized basalts/SWCNT composites' powders at SWCNT ratios of 0, 1, 3, and 5 wt% at 2θ range of (**a**) 5-80°, (**b**) 35-37°, and (**c**) 47-50°
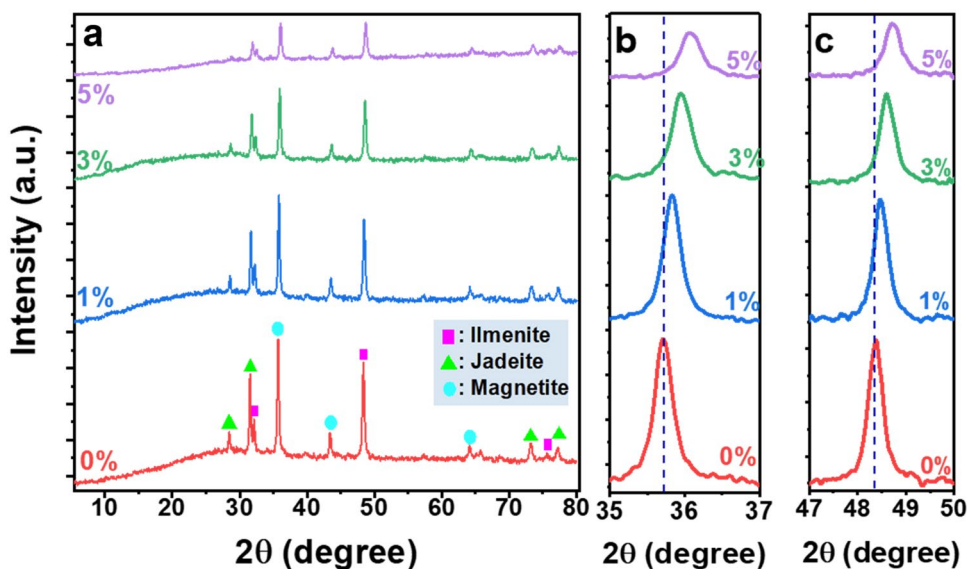
the recorded XRD patterns using the Rietveld method. The ICDD (PDF-2/Release 2011 RDB) card no 01–078-2037 was the best fit and match with diffraction peaks at 2θ values of 28.47, 31.53, 73.14, and 77.14°. According to this card number, these diffraction peaks were respectively indexed to the (021), (310), (313), and (640) planes corresponding to the jadeite ($Ca_{0.29}Na_{0.6}Al_{0.75}Mg_{0.21}Fe_{0.08}(Al_{0.01}\,Si_{1.99}\,O_6)$) that has the monoclinic crystal system with symmetry of C12/c1 space group. While the ICDD (PDF-2/Release 2011 RDB) card no 01–070-6273 was the best card to fit and match with diffraction peaks at 2θ values of 32.11, 48.38, and 75.65° that were indexed to (104), (024), and (036) planes correspond to the ilmenite ($FeTiO_3$), which has the trigonal crystal system with the symmetry of R $\bar{3}$ space group. Besides, the ICDD (PDF-2/Release 2011 RDB) card no 01-071-6338 was the best card to fit and match with diffraction peaks at 2θ values of 35.68, 42.9, and 62.99° indexed to (311), (400), and (440) planes correspond to the magnetite (Fe_3O_4) [37–39] that has the cubic crystal system with the symmetry of Fd $\bar{3}$ m space group. Accordingly, the XRD results indicated the presence of three different crystalline mineral phases that were included in the pure basalts. The XRD patterns for the prepared composites at the SWCNT ratios 1, 3, and 5 wt% showed nearly the same

diffraction peaks, but two main differences can be noticed. The first difference is that their diffraction peaks' intensities decreased as the SWCNT ratio increased. The second difference is that the diffraction peaks at 2θ values of 35.68 and 48.38°, which belong respectively to magnetite and ilmenite, shifted to higher values of 2θ while increasing the SWCNT. The decrease in the intensity and the shift in the diffraction peaks of the XRD pattern could be due to two parameters. Firstly, the sonication (4 hours) could induce amorphization in the crystal phase [40] of the nano basalts powders. Secondly, the tiny ratio of the amorphous carbon in the SWCNT increases while increasing the SWCNT ratio; it could play a significant role in the impurity phase formation during the nanocomposites preparation; leading to the decrease and shift in the XRD peak patterns. We summarized the obtained results from the XRD in Table 2. The ratio of jadeite is 70% (jadeite is a pyroxene mineral. Here, pyroxene and plagioclase feldspar make up the predominantly basalts.

Raman and FTIR spectroscopy is a non-destructive and reliable method to characterize different molecules, such as geomaterials [41] or biomaterials [42]. Generally, Raman and FTIR spectra are used to identify the species by comparison with the spectra published that belong to the same species. Figure 4a and b display the Raman and FTIR spectra,

Table 2 The recorded crystal structural phases, phase ratios, lattice parameters, and space groups in basalt via XRD analysis

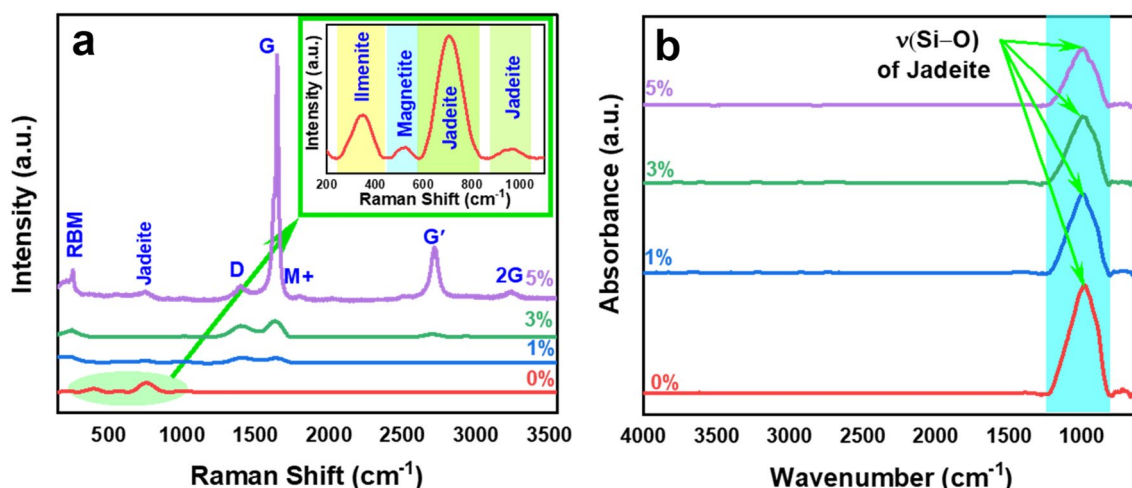| Crystal phase	Chemical formula	Lattice parameters (Å)			Space group	Ratio (%)	Crystallite size (Å)
		a	b	c			
Jadeite	$Ca_{0.29}Na_{0.6}Al_{0.75}Mg_{0.21}Fe_{0.08}(Al_{0.01}\,Si_{1.99}\,O_6)$	9.4704	8.6261	5.2211	C12/c1	70 ± 9	500 ± 25
Ilmenite	$FeTiO_3$	5.1002	5.1002	14.3516	R $\bar{3}$	9 ± 13	784 ± 33
Magnetite	Fe_3O_4	8.3363	8.3363	8.3363	Fd $\bar{3}$ m	21 ± 4	16.8 ± 4

Fig. 4 **a** Raman spectra **b** FTIR spectra of nanosized basalts/SWCNT composites' powders at SWCNT ratios 0, 1, 3, and 5 wt.%; the inset figure is the zooming in of the nanosized basalts Raman spectral range 200–1100 cm-1

respectively, of the nanosized basalts/SWCNT composites' powders at the SWCNT ratios 0, 1, 3, and 5 wt%. Different peaks can be seen in the Raman spectra (Fig. 4a), where the Raman spectrum of pure nanosized basalts (SWCNT ratio is 0 wt%) displayed weak peaks in the Raman spectral region of 200–1100 cm^{-1}. Therefore, we zoomed in on this spectral region, as shown in the inset figure of Fig. 4a. This inset figure exhibits four peaks in the Raman spectral regions of 250–440, 460–580, 600–840, and 900–1050 cm^{-1}, reflecting the mineral characterization of the pure nanosized basalts. The Raman peak in the spectral region 250–440 cm^{-1} centered at 339 cm^{-1} could be referred to as the E_g symmetry resulting from the TiO_6 octahedra translation vibration belonging to the ilmenite [43]. While the peak in the Raman spectral region 460–580 cm^{-1}, which is located at 528 cm^{-1}, might be attributed to mode T_{2g} resulting from the asymmetric stretch vibration of Fe–O belonging to the magnetite [44]. The third and fourth peaks in the Raman spectral regions 600–860 and 900–1050 cm^{-1}, which were centered at 700 and 978 cm^{-1}, respectively, were attributed to symmetric vibration resulting from the bridging (Si–O-Si) of SiO_4 in the jadeite mineral phase [45]. The Raman spectrum of the nanosized basalts/SWCNT composites' powders at the SWCNT ratios 1, 3, and 5 wt% show new peaks. These peaks are centered at 207, 1350, 1595, 1758, 2678, and 3189 cm^{-1}; they started appearing while adding the SWCNT and increased with increasing its ratio, becoming predominant peaks at the SWCNT ratio of 5 wt%. There is a low-energy band between ~120 and ~220 cm^{-1} including a sharp peak at 207 cm^{-1} which characterizes the radial breathing mode (RBM) [46]. The Raman scattering value of the RBM peak indicated the diameter of SWCNT is ~ 1.19 nm; this value is in good agreement with the value reported in the datasheet from the manufacturer. The other peaks are attributed respectively to peaks D, G, M +, G′, and 2G of the SWCNT [46, 47]. We recorded the Raman

spectrum of the pristine SWCNT, which showed very high intensity compared with nanosized basalts/SWCNT composites' powders nanosized; we compared the pristine SWCNT with the nanosized basalts/SWCNT composites' powder at the SWCNT ratio of 5 wt.% as shown in Fig. S4. From the Raman spectra in Fig. 4a and Fig. S4, although the ratios of the SWCNT are minor (the maximum ratio was 5 wt%), the Raman features of the nanosized basalts/SWCNT composite at 5 wt% become nearly like the Raman features of the pristine SWCNT, only with less intensity.

FTIR spectra of the pure nanosized basalts and basalts/SWCNT composites' powders at the SWCNT ratios 1, 3, and 5 wt% are displayed in Fig. 4b. This figure shows that the FTIR spectra of the basalts/SWCNT nanocomposites' powders showed almost the same signature. They all demonstrated a strong absorption peak in the FTIR spectral range 1230–800 cm^{-1}; this peak was attributed to jadeite's Si–O stretch mode (bridged) and (non-bridged) [48]. The increase in SWCNT ratios did not show significant changes in FTIR spectra compared with the pure basalt's nanosized FTIR spectrum (Fig. 4b). Only a slight decrease in the peak intensity can be noticed with the increase of the SWCNT ratio.

3.2 Thermal Analysis

The thermal analysis results for the pure nanosized basalts and the basalts/SWCNT nanocomposites' powders at the SWCNT ratios 1, 3, and 5 wt.% are presented in Fig. 5. DSC and TGA curves of the pure basalts are plotted in Fig. 5a; the DSC curve shows nearly constant values, suggesting no crystal phase has changed in the pure basalts while heating them in the temperature range starting from room temperature up to 1200 Kelvin. Also, the TGA curve of pure basalts seems to have constant values, indicating basalts' thermal stability. Although the pure nanosized basalts mass ratio was 98.66% at 1200 Kelvin, showing 1.34% is the loss ratio in
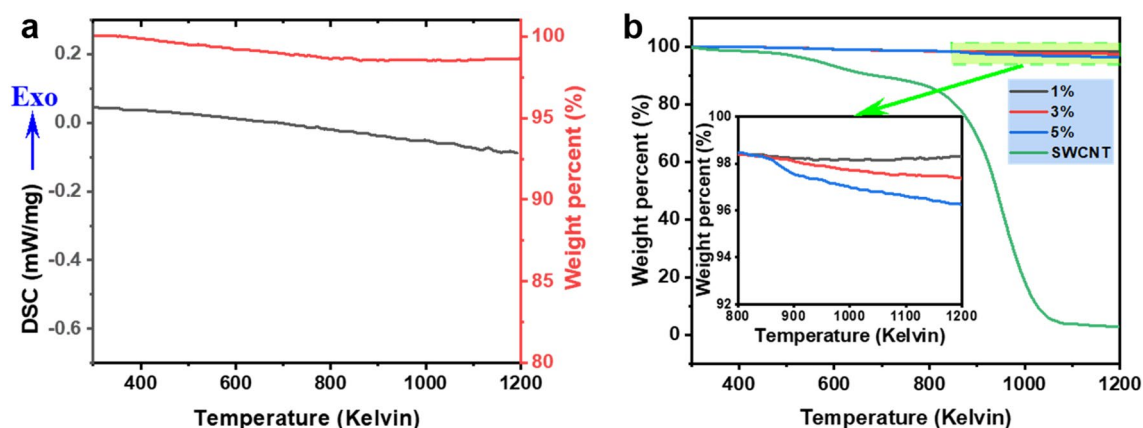

Fig. 5 Thermal analysis (**a**) DSC and TGA of pure nanosized basalts (**b**) TGA of pristine SWCNT and basalts/SWCNT nanocomposites' powders at SWCNT ratios 1, 3, and 5 wt%; the inset figure is the zooming in of the TGA in the temperature range of 800–1200 Kelvin

the mass. However, this lost mass could be ascribed to the trapped gases, which could release and come out of basalts during thermal heating [27]. In general, the pure nano basalts showed thermal stability being the basalts are volcanic rocks formed under high temperatures from the cooling of lava. Figure 5b displays the TGA curves of the nanosized basalts/SWCNT composites' powders at the SWCNT ratios 1, 3, and 5 wt%, besides the pristine SWCNT. The TGA curve of the pristine SWCNT shows two steps. The first step was small in the temperature range of 500–690 Kelvin; at the end of this step, the pristine SWCNT mass ratio decreased to 90%. The second step was prominent in the temperature range 730–1080 Kelvin; the mass ratio of the SWCNT was 3.95% at the end of this step. The pristine SWCNT mass ratio recorded 2.9% at 1200 Kelvin. The small and large steps in the TGA curve of the pristine SWCNT curve could be attributed to the combustion of amorphous and graphitic carbon, respectively [49]. The first step was small could be due to a small amount ratio of the amorphous carbon in the SWCNT. The TGA curves of nanosized basalts/SWCNT

composites' powders at the SWCNT ratios 1, 3, and 5 wt% showed constant values with slight decreases after heating beyond 800 Kelvin (Fig. 5b). We zoomed in on this range, as shown in the inset figure. The mass ratio declined to 98.31, 97.36, and 96.26% at 1200 Kelvin for the prepared nanocomposites at the SWCNT ratios 1, 3, and 5 wt%, respectively. The decreases in the mass ratios with increasing the SWCNT ratio could come from the combustion of SWCNT content, as we already observed in the TGA curve of the pristine SWCNT.

3.3 Electrical Properties

The temperature dependence of electrical conductivity of the prepared nanosized basalts/SWCNT composites' electrical properties at SWCNT ratios 0, 1, 3, and 5 wt% was investigated by studying the ac conductivity at a wide range of temperatures and different applied electrical frequencies. Figure 6(a–d) displays the electrical conductivity as a function of 1000/temperature in Kelvin (T) for all nanosized basalts/
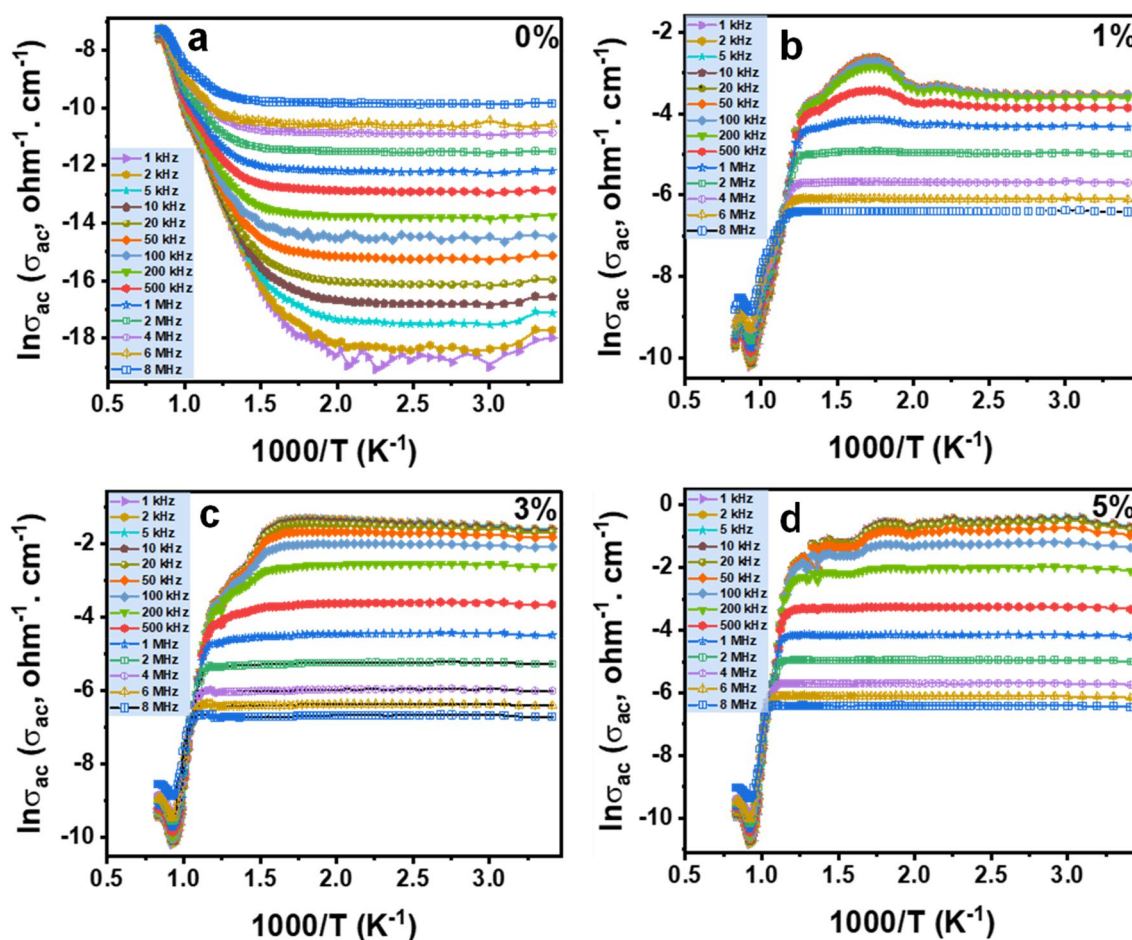

Fig. 6 Electrical conductivity of the prepared nanosized basalts/SWCNT composites at SWCNT ratios 0, 1, 3, and 5 wt% versus 1000/T at different applied electrical frequencies

SWCNT composite samples. It can be noticed that the electrical conductivity of pure basalt nanosized (SWCNT ratio is 0 wt%) showed two behaviors. The first behavior is insulating, where the pure basalt nanosized demonstrated low conductivity values and was nearly constant while increasing the temperature, indicating stable electrical behavior in the temperature range starting from RT up to 600 Kelvin. The second behavior is the semiconducting behavior; here, the pure basalt nanosized demonstrated gradually increased electrical conductivity with increasing temperature, suggesting the pure basalt nanosized is thermally activated at higher temperatures. The first behavior could be understood because the thermal energy could be insufficient to liberate electrical carrier charges. In the second behavior, the thermal energy is enough to release and liberate more carriers at higher temperatures [25, 30]. Interestingly, although nanosized basalts/SWCNT composites at SWCNT ratios of 1, 3, and 5 wt% showed two behaviors, they are entirely different even at the lowest ratio of the SWCNT; they are upside down compared with the two behaviors of the pure basalts. The first behavior is that they showed excellent and stable electrical conductivity in the temperature range, starting from RT to 800 Kelvin. The second behavior is that they demonstrated decreased electrical conductivity values with the increasing higher temperature nearly greater than 800 Kelvin. The first behavior is considered metallic, which agrees with Gabal [50] and Salah [29], where the electrical conductivity is roughly constant with increasing temperature. This behavior is an original feature of the single-wall and multi-wall carbon nanotubes (CNT) [51]. From the point of the electrical properties, these results suggest that SWCNT enhances the electrical conductivity of the nanosized basalts/SWCNT composites and makes them behave like conductors. The second behavior was where the electrical conductivity decreased at higher temperatures beyond 800 Kelvin. This result can be understood through the SWCNT thermal stability, where the SWCNT starts the thermal dissociation process at higher temperatures [50]. Therefore, the nanosized basalts could be responsible for electrical conductivity in the second region beyond 800 Kelvin (the nanosized basalts showed low conductivity).

The frequency dependence of electrical conductivity of all nanocomposites was investigated and shown in Fig. 7(a–d). The conductivity was plotted as a function of natural logarithms of the applied electrical frequency at different temperatures. From this figure, it can be noticed that the electrical conductivity of the pure basalt nanosized showed gradual increases with the increasing frequency at the lower temperatures (frequency-dependent). Besides, it showed stable values (almost horizontal linear behavior) with increasing frequency at higher temperatures (frequency-independent). These results could indicate the change in the conduction mechanism [52–54], where the correlated

barrier hopping (CBH) model could describe the conduction mechanism [30]. In this model, single polaron CBH dominates the electrical transport mechanism at higher temperatures, while, at lower temperatures, the bipolaron CBH mechanism controls the electrical conduction mechanism [55]. Besides, Fig. 7(b–d) shows the electrical conductivity dependence on frequency for all nanosized basalts/SWCNT composites at SWCNT ratios 1, 3, and 5 wt%. These nanocomposites demonstrated different behavior than the pure nanosized basalts. At low temperatures, they showed roughly constant high electrical conductivity values with increasing the frequency up to 200 kHz; then, they showed a decreasing electrical conductivity with increasing the frequency after 200 kHz. The Drude model can illustrate this result, which describes the alternative current electrical conductivity as it decreases with the frequency [56], where the charge carriers cannot follow the fast changeable frequencies (high frequencies) [57].

Figure 8 exhibits the impact of SWCNT in the nanosized basalts at SWCNT ratios 0, 1, 3, and 5 wt%. The temperature dependence of electrical conductivity at the frequency of 20 kHz is shown in Fig. 8a for all the nanosized basalts/SWCNT composites at SWCNT ratios 0, 1, 3, and 5 wt%. At the same time, the frequency dependence of the electrical conductivity is exhibited in Fig. 8b at 500 Kelvin. At the frequency of 20 kHz, the electrical conductivity of nanocomposites at temperatures of 300 and 1000 K was listed in Table 3. These results (Fig. 8 and Table 3) display how the SWCNT changed and enhanced the nanosized basalts' electrical conductivity values and electrical behavior. These results could suggest that introducing the SWCNT into the nanosized basalt has generated and increased the appropriate passageways to transport more charge carriers [58].

3.4 Dielectric Properties

The temperature dependence of the dielectric constants and dielectric losses for all nanosized basalt/SWCNT composites were estimated at different applied electrical frequencies. Their results are shown in Fig. 9(a–d) and Fig. 10(a–d), respectively. The pure basalts' dielectric constant and dielectric loss showed constant lower values at lower temperatures, ranging from RT to 800 Kelvin. This result could indicate that the contributions of all polarizations are weak and constant. In this temperature range, it can be said that the dielectric constants and dielectric losses are temperature-independent. While its dielectric constant and dielectric loss exhibited gradually increasing values with gradually increasing the temperature range beyond 800 Kelvin. Here, in the temperature range beyond 800 Kelvin, the dielectric constant and dielectric loss become temperature-dependent. The thermal energy could become enough to create more localized
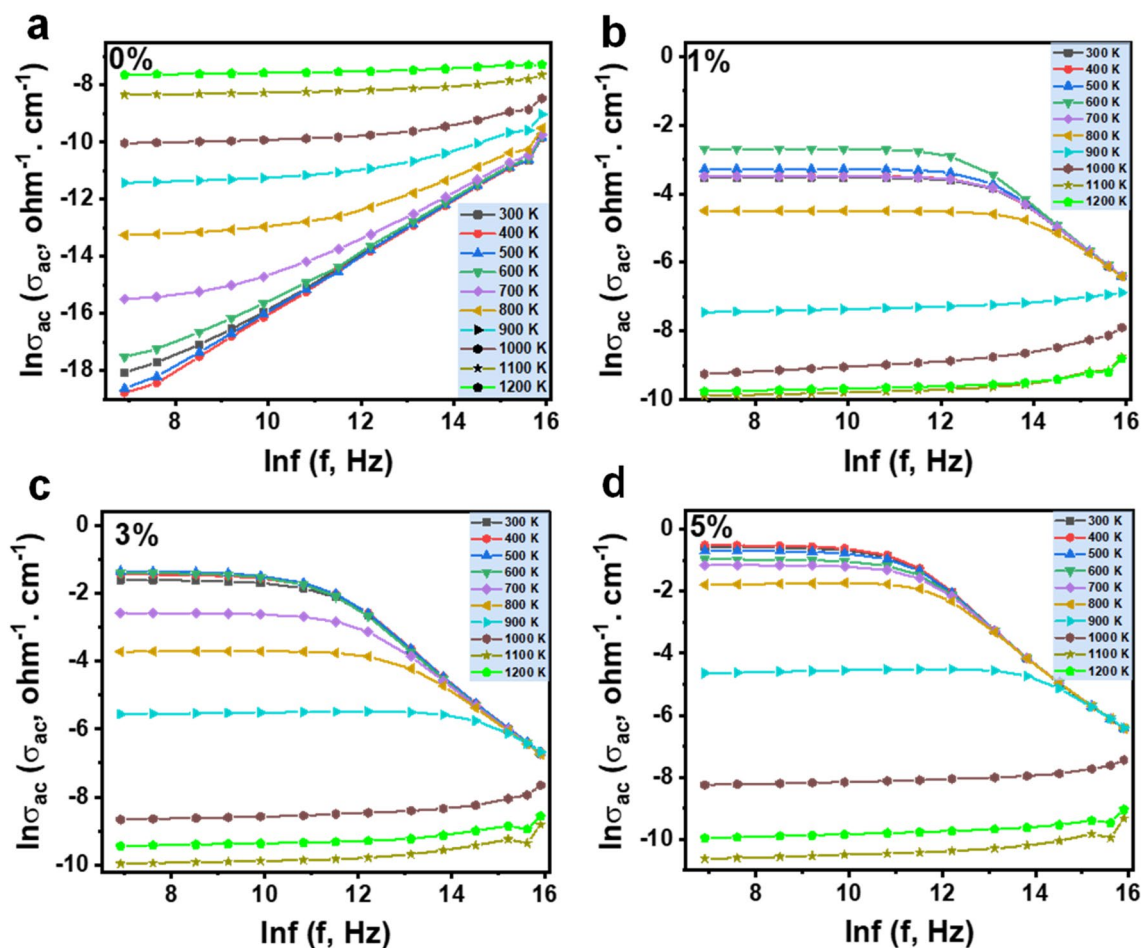
Fig. 7 Electrical conductivity of the prepared nanosized basalts/SWCNT composites at SWCNT ratios of 0, 1, 3, and 5 wt% versus the natural logarithm of electrical frequency at different temperatures
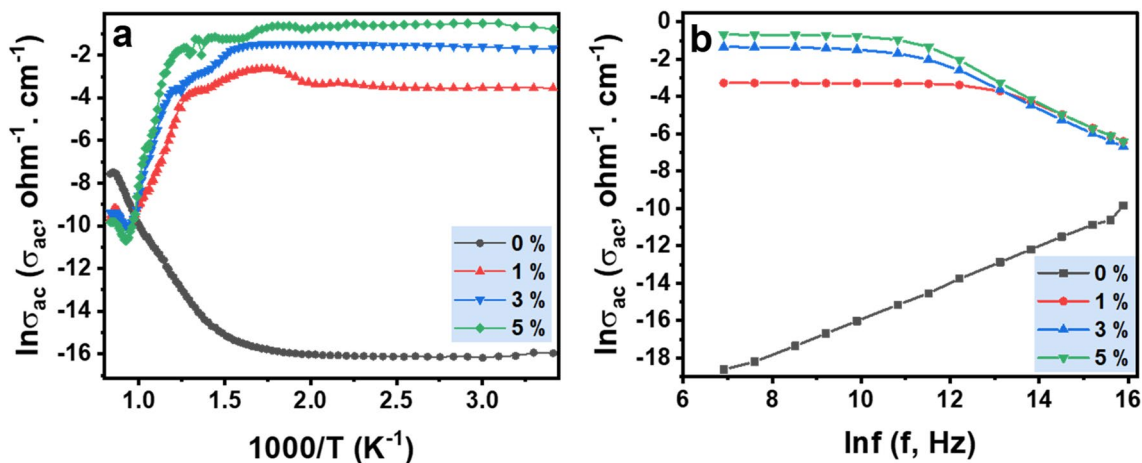

Fig. 8 Electrical conductivities of the nanosized basalts/SWCNT composites at SWCNT ratios 0, 1, 3, and 5 wt%, **a** the temperature dependence of electrical conductivity at 20 kHz, **b** the frequency dependence of electrical conductivity at 500 Kelvin

Table 3 The electrical conductivities, the dielectric constants, the dielectric losses of the nanosized basalts/ SWCNT composites at SWCNT ratios of 0, 1, 3, and 5 wt% at temperatures of 300 and 1000 Kelvin and the frequency of 20 kHz

SWCNT ratio (%)	σ $(\Omega.cm)^{-1}$		ε'		ε''	
	RT	1000 K	RT	1000 K	RT	1000 K
0	1.16×10^{-7}	4.93×10^{-5}	10.45	388.05	2.44	4.31×10^{3}
1	0.03	1.17×10^{-4}	3.86×10^{4}	1.22×10^{3}	1.29×10^{6}	1.02×10^{4}
3	0.19	1.88×10^{-4}	2.01×10^{5}	1.60×10^{4}	2.51×10^{6}	2.00×10^{4}
5	0.46	2.89×10^{-4}	2.65×10^{5}	1.84×10^{4}	3.79×10^{6}	1.60×10^{4}
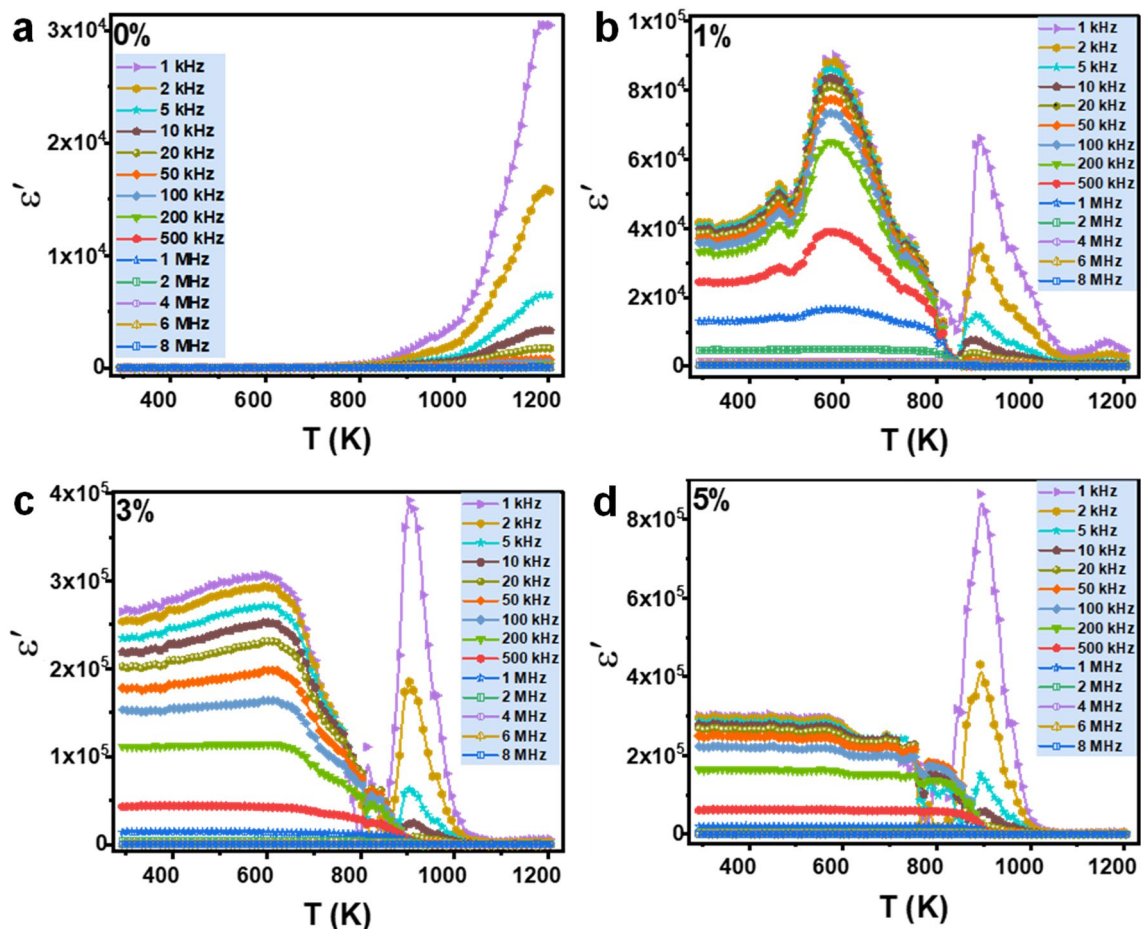
Fig. 9 Dielectric constants with the absolute temperature for the nanosized basalts/SWCNT composites at SWCNT ratios 0, 1, 3, and 5 wt% and different frequencies

dipoles from their atomic bonds, thus raising the number of dipoles and increasing polarization [59].

The nanocomposites at SWCNT ratios 1, 3, and 5 wt% and different frequencies showed entirely different behavior than the pure nanosized basalts. They showed higher stable values for both the dielectric constants and the dielectric losses at lower temperatures. Then, they exhibited gradually decreased values with a further increase in the temperature; this decrease could be explained through the thermal dissociation process of SWCNT at higher temperatures. Besides, they showed a relaxation peak at 900 Kelvin. This relaxation

peak was not seen in the pure nano basalts, which means this peak is connected with SWCNT addition. Therefore, it can explain this peak through the thermal analysis, mainly the TGA curve of the SWCNT. Where the graphitic structure of the SWCNT breaks down under the thermal energy in the temperature range between 730 and 1080 Kelvin (see Sect. 3.2). Therefore, this peak could occur due to SWCNT's thermal dissociation process. Where the SWCNT could dissociate into the carbon atoms that bond to the oxygen atoms forming CO and CO_2 molecules [60]. Therefore, at this temperature range, i.e., 730–1080 Kevin, the CO and CO_2 could
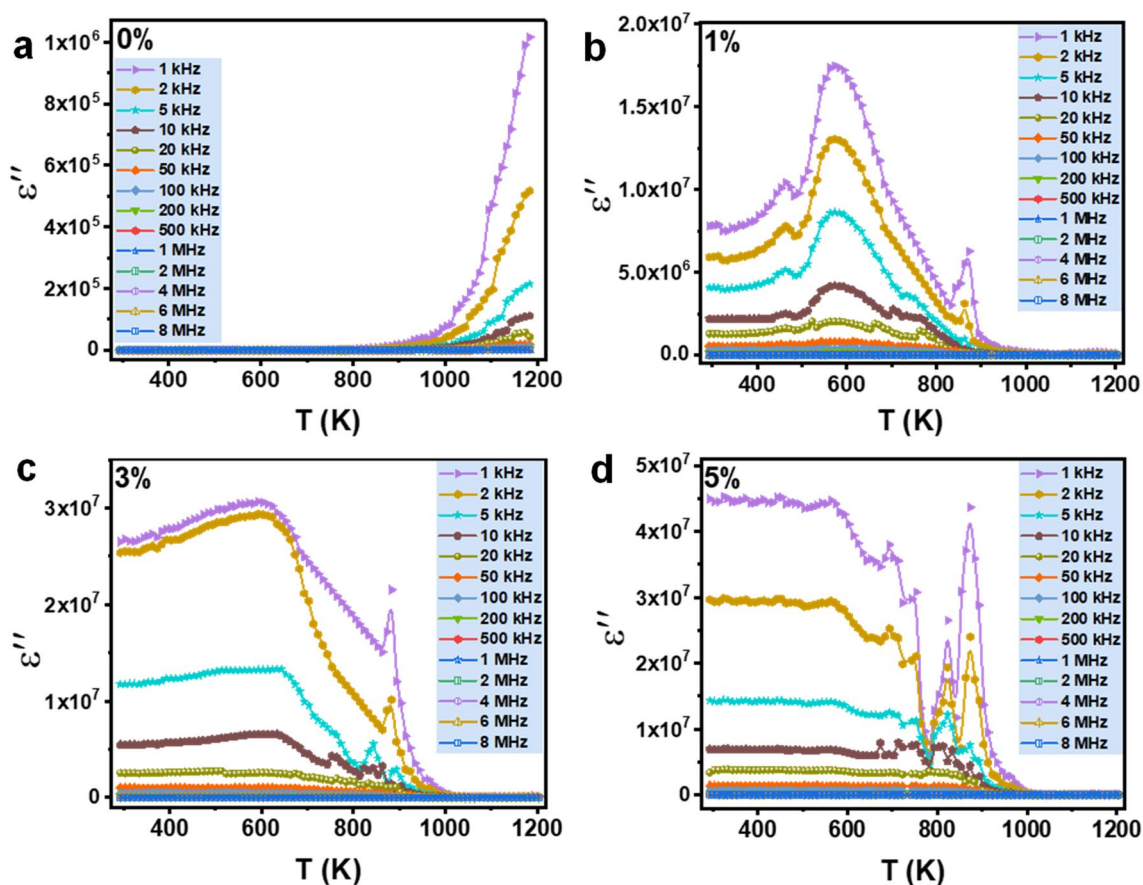
Fig. 10 Dielectric losses with the absolute temperature for the nanosized basalts/SWCNT composites at SWCNT ratios 0, 1, 3, and 5 wt% and different frequencies

accumulate inside the nanocomposites, causing increases in the dipolar or orientation polarization that could finally lead to a sudden increase in the dielectric properties of the basalts/SWCNT nanocomposites where it was reported that the dielectric properties of wheat gluten increased linearly with treatment by CO_2 [61]. Later, the CO and CO_2, as gases, started to escape and liberate from the nanocomposites; therefore, dropping in the dielectric properties; this means, after SWCNT decomposition, the behaviors of the basalts that have low dielectric properties, become dominant.

The frequency dependence of the dielectric constants and dielectric losses for the nanosized basalt/SWCNT composites at SWCNT ratios 0, 1, 3, and 5 wt% were investigated at different temperatures and exhibited in Fig. 11(a–d) and Fig. 12(a–d), respectively. The pure basalts' dielectric constant and dielectric loss pretended stable higher values at lower frequencies and gradually decreased with increasing the frequencies regardless of the temperature. This feature could be a typical feature at high frequencies; it is difficult for all dipoles to follow the fast changeable electric field, leading to lagging in ordering the dipoles and subsequently low dielectric values. While

frequency dependence of the dielectric constants of the nanosized basalt/SWCNT composites at SWCNT ratios 1, 3, and 5 wt% show high values of dielectric constant with two behaviors regarding the temperature (Fig. 11b–d). The first behavior is in the curves representing temperatures up to nearly 800 Kelvin. In this behavior, the composites' dielectric constant showed high values and stable character (frequency-independent); then, they decreased with the increasing frequency. The second behavior is in the curves for temperatures beyond 800 Kelvin; these curves show low and decreased dielectric constant and dielectric loss values. The first behavior could result from the existence of SWCNT that can enhance the dielectric properties of the composites [62, 63]. In contrast, the second behavior could result from the nanosized basalts responsible for the composites' dielectric properties after the SWCNT thermal dissociation process. It can also observe as the concentration of the SWCNT increased as the dielectric constant and dielectric loss values increased (Table 3, Fig. 11, and 12). Jonscher theory, Maxwell–Garnett theory, and the percolation threshold are theories that can be applied to study the relationship between the dielectric properties of
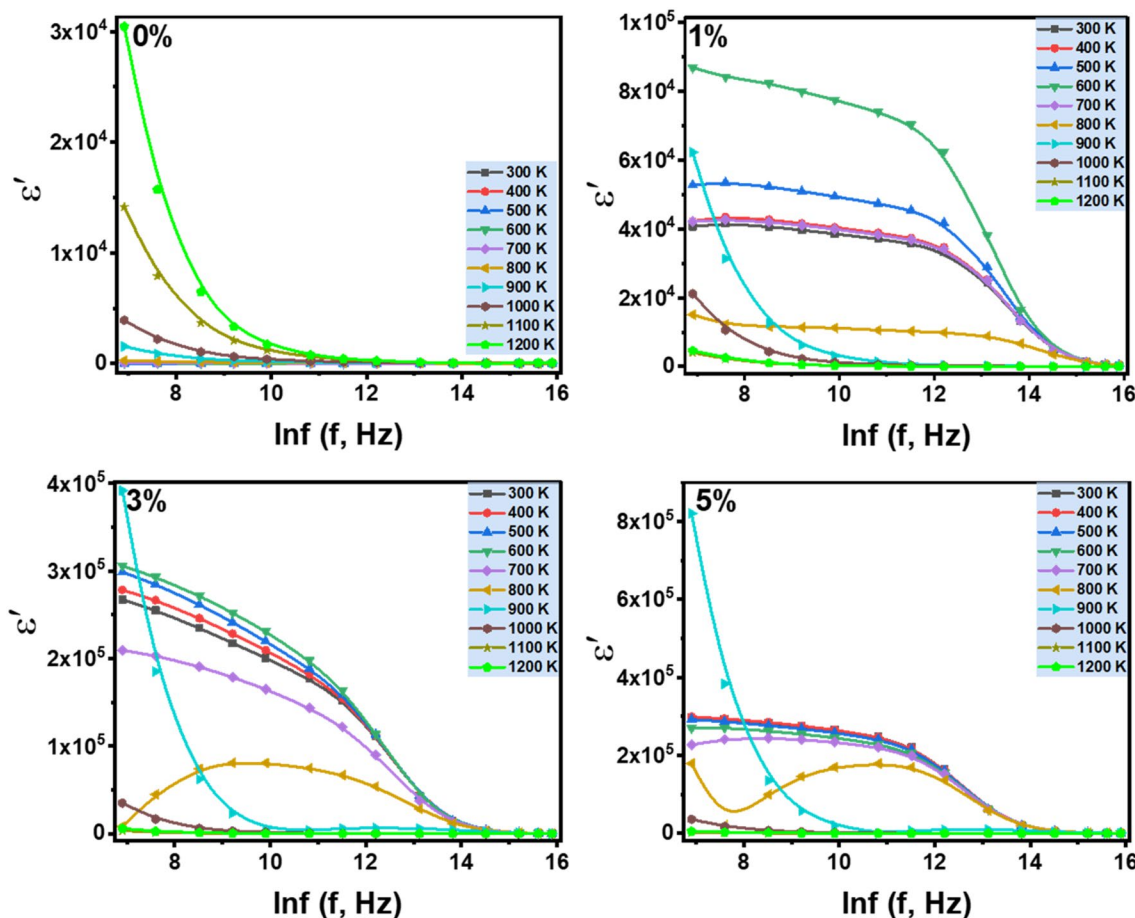
Fig. 11 Dielectric constants with the logarithm of frequency for the nanosized basalts/SWCNT composites at SWCNT ratios 0, 1, 3, and 5 wt% and temperatures

the composite and the concentration of the filler material in the composite [62]. The percolation threshold theory was used for studying the CNT/polymer composites [62, 63]. Accordingly, we used this model to study basalts/SWCNT nanocomposites. Based on this model, at the temperature of 400 Kelvin and frequency of 500 kHz, the obtained experimental results were fitted to the power-law using the following equation [62, 63]:

$$\varepsilon_{\text{eff}} = \varepsilon_{\text{SWCNT}} (f - f_c)^s \quad f > f_c \tag{8}$$

where ε_{eff} and $\varepsilon_{\text{SWCNT}}$ are the composites' and SWCNT effective dielectric constants, f_c is the percolation threshold, f_{SWCNT} is the SWCNT ratio, and S is the critical exponent. The obtained S value was 0.93, which lay in the range of this model (0.8–1) at f_c of 0.5 wt%. The percolation threshold value discussed the significant increase in the dielectric constant even at the basalts/SWCNT nanocomposites with SWCNT of ratio 1 wt%. The dielectric loss showed nearly the same behavior, but it decreased gradually with increasing the frequency but no frequency-independent part (Fig. 12).

The nanosized basalt/SWCNT composites' dielectric constants and dielectric loss are exhibited in Fig. 13 and 14, respectively. The temperature dependence of dielectric constant and dielectric loss at 20 kHz are shown in Fig. 13a and 14a, respectively; simultaneously, the dielectric constant and dielectric loss frequency dependence are exhibited in Fig. 13b and 14b at 500 Kelvin. From these figures, the dielectric constant and dielectric loss of the composites are outstandingly increased for the composites; it can also be noticed that their values increased as the SWCNT ratio increased. For instance, at 20 kHz, the dielectric constant of nanosized basalt/SWCNT composites at SWCNT ratios 0, 1, 3, and 5 wt% recorded 10.45, 3.86×10^4, 2.01×10^5, and 2.65×10^5, respectively, at the RT (Table 3). It was reported that the conducting CNT creates conducting panicles isolated by dielectric layers of the host in the composite [62, 63] (in our state, the bundles and nets of the SWCNT act like the conducting panicles while nanosized basalts act like the dielectric layers of the host). Where the conducting panicles do like many mini capacitors, the polarization effects between the conducting panicles themself can
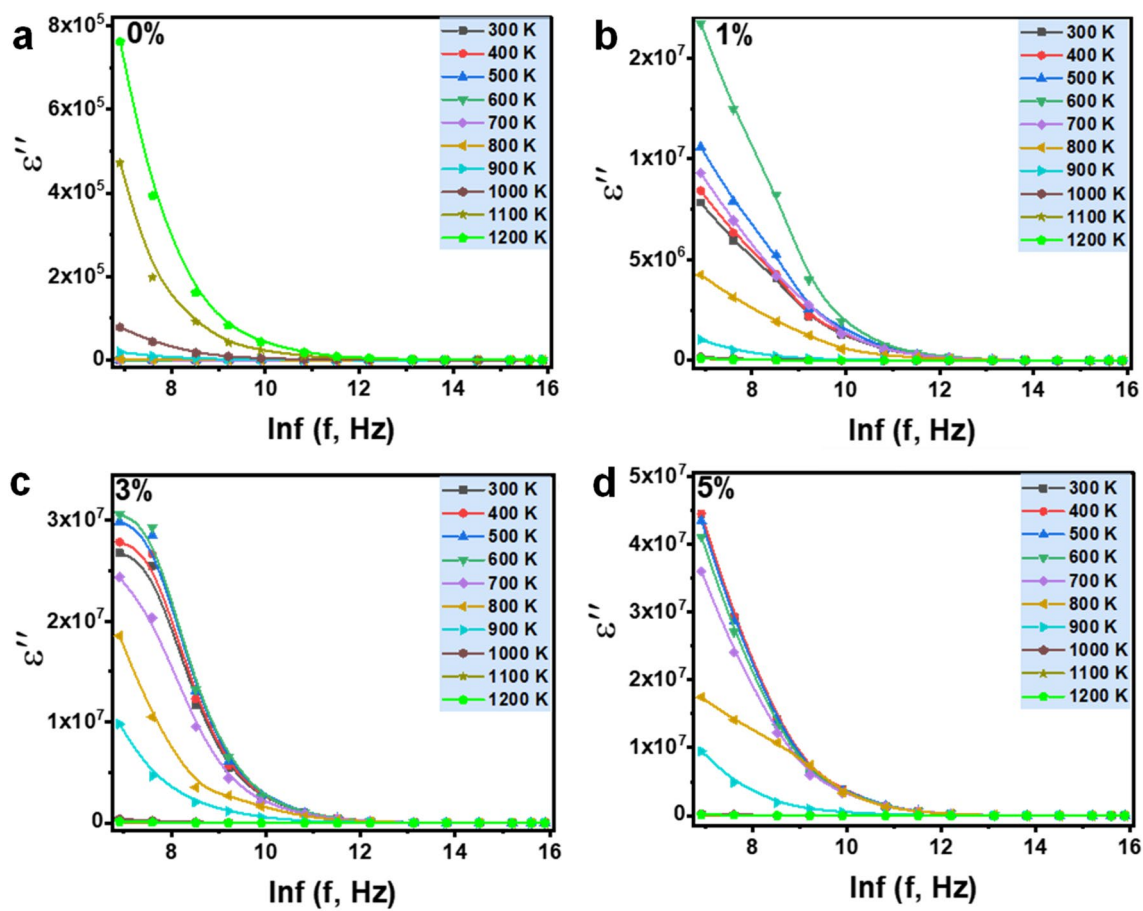
Fig. 12 Dielectric losses with the logarithm of frequency for the nanosized basalts/SWCNT composites at SWCNT ratios 0, 1, 3, and 5 wt% and temperatures
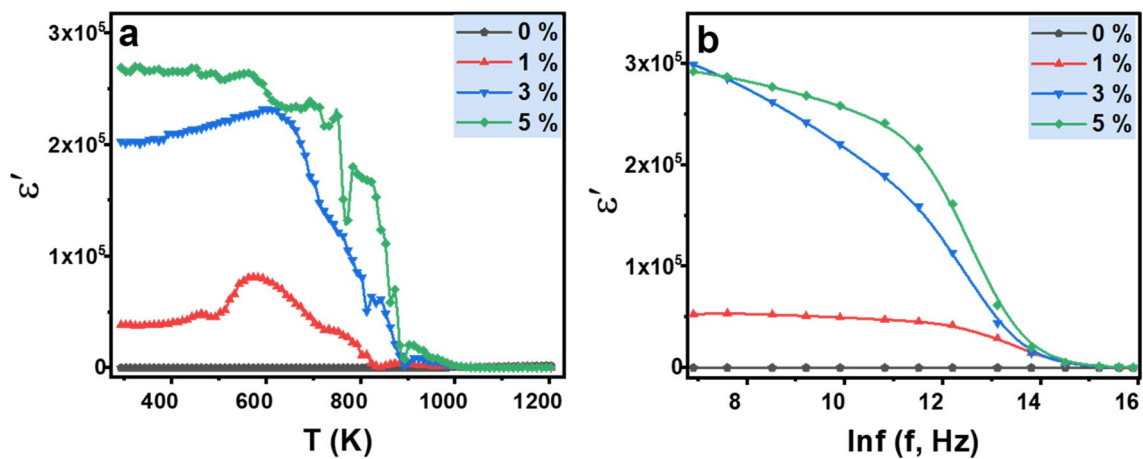

Fig. 13 The dielectric constant of nanosized basalts/SWCNT composites at SWCNT ratios of 0, 1, 3, and 5 wt%, **a** the temperature dependence of dielectric constant at 20 kHz, **b** the frequency dependence of dielectric constant at 500 Kelvin

enhance the storage of energy and, therefore, the dielectric properties [62, 63]. Besides, the interfacial polarization was reported to increase while adding nanofibers to the host material in the composites, causing enhancements in the dielectric performances. Here, in our nanocomposites, the interfacial polarization between the nano basalts and the
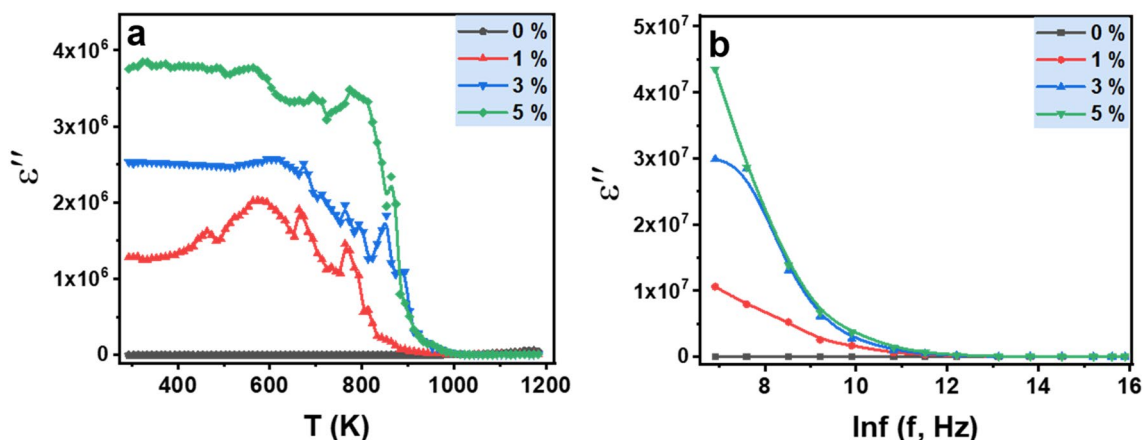
Fig. 14 The dielectric loss of nanosized basalts/SWCNT composites at SWCNT ratios 0, 1, 3, and 5 wt%, **a** the temperature dependence of dielectric loss at 20 kHz, **b** the frequency dependence of dielectric loss at 500 Kelvin

SWCNT could increase, enhancing the dielectric properties of the prepared nanocomposites. This illustration could be a reasonable reason for the significant improvement in the dielectric properties of the nanosized basalt/SWCNT composites. The decrease in the dielectric properties at higher frequencies could be understood through dielectric relaxation at higher frequencies since the dielectric polarization cannot follow the applied changeable direction electric field at high frequency [64], leading to the decrease in the dielectric performance.

3.5 EMI Shielding Performance

The adding SWCNT into the nano basalts enhanced the electrical conductivity and dielectric constants significantly; these materials are candidate materials for EMI. The electrical conductivity of materials must be higher than 1 S/m to achieve a premium EMI shielding performance. The pure (raw) nano basalts showed electrical insulator behavior ($\sigma << 1$ S/m); while the prepared nanocomposites of

basalts/SWCNT at SWCNT ratios 1, 3, and 5 wt% showed electrical conductivities of more than 1 S/m (see Figs. 6, 7, and 8). Accordingly, the nanocomposites could be utilized as EMI shielding materials. Based on Simon's formulas, the capability of the materials for EMI shielding follows its electrical conductivity, thickness, and frequency [35]. We utilized these formulas (see Eqs. 5–7) to estimate the EMI shielding ability of the prepared basalts/SWCNT nanocomposites with a thickness of 2 mm at the X-band; the obtained EMI shielding results are shown in Fig. 15(a–c). It can be observed that the SE_A showed more EMI shielding performance (Fig. 15a) compared with EME SE_R. Besides, SE_A values showed an upward trend with the increase the frequency. For instance, at 8 GHz, they were 16.7, 34.3, and 61.6 dB for the nanocomposites with SWCNT content of 1, 3, and 5 wt.%, respectively (Fig. 15a); they increased to 20.4, 42.6, and 74.5 dB at 12 GHz. At the same time, SE_R values showed a downward trend with the increase the frequency. They were 5.7, 12.1, and 13.9 dB at 8 GHz for the nanocomposites with SWCNT content of 1, 3, and 5 wt%,
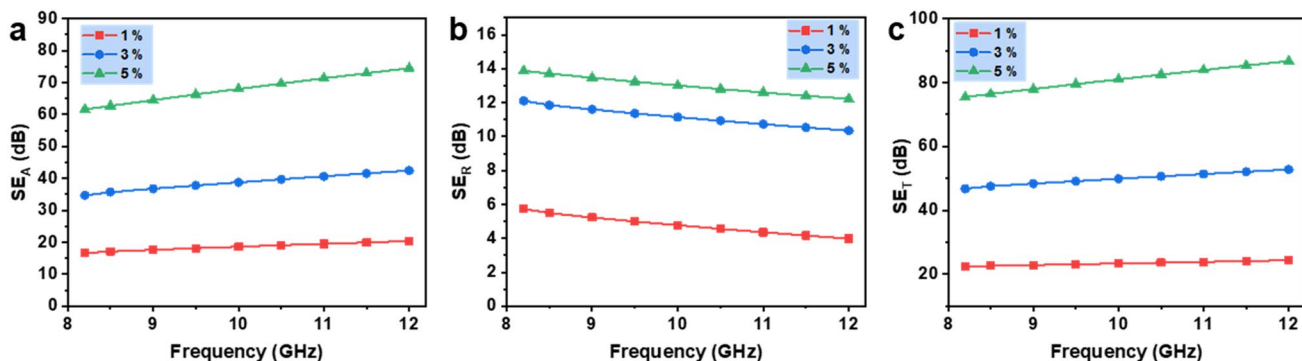

Fig. 15 SE for a 2 mm thickness of the basalts/SWCNT nanocomposites at SWCNT ratios of 1, 3, and 5 wt% versus the frequency of the X-band. **a** SEA, **b** SER, **c** and **d** SET

respectively (Fig. 15b); with increases in the frequency, they decreased to be 4, 10.3, and 12.2 dB at 12 GHz. The enhancements in SE_A values lead to considerable improvements in the EMI total SE as seen in Fig. 15c.

SE_A, SE_R, and SE_T for a 2 mm thickness of the basalts/SWCNT nanocomposites as a function of the SWCNT content at 10 GHz are displayed in Fig. 16. Their values manifested an apparent upward trend with the increase of SWCNT content; it can be observed that the SE_A and SE_T of the prepared basalts/SWCNT nanocomposites got considerably enhanced while increasing the SWCNT ratio. For instance, the SE_T value was 23.4 dB for nanocomposite with SWCNT content of 1 wt% that increased to 81 dB with SWCNT content 5 wt%. The increase in the total EMI SE values could be ascribed to increasing the electrical conductivity with increasing SWCNT content (Figs. 6, 7, and 8). It can notice that all the prepared basalts/SWCNT nanocomposites showed SE_T values that are larger than 20 dB (Fig. 16), which means these nanocomposites can prevent 99% of the incident electromagnetic energy in the range of the X band [65]. Moreover, the basalts/SWCNT nanocomposites with the SWCNT ratio of 3 and 5 wt% recorded the SE_T value of more than 30 dB, which means this nanocomposite can block 99.9% of the electromagnetic energy [66]. The SE_T of the prepared nanocomposite with SWCNT content of 5 wt% recorded 81; it is higher than 60 dB, which means more than 99.9999% of electromagnetic energy can be shielded; in other words, only less than 0.0001% of electromagnetic energy that can penetrate [66] through 2 mm thickness of these nanocomposites. The EMI results for the prepared basalts/SWCNT nanocomposites proved the X band's excel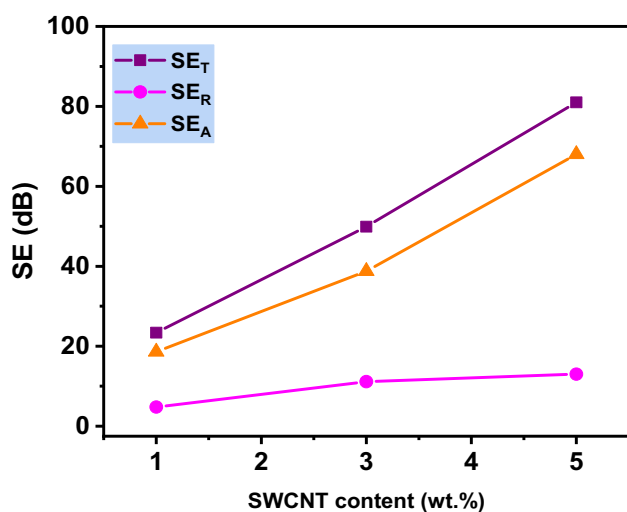lent EMI shielding performance. This band is considered one of the radar-frequency bands that has become a threatening frequency for equipment and weapons.

4 Conclusion

Here, we investigated the electrical and dielectric properties of the pure nanosized basalts and nanosized basalts/SWCNT composites. We prepared nanosized basalts from the basalt rocks using the ball milling technique. EDS and XRD showed respectively the elemental composition and the mineral phases' structure included in the pure basalts and their prepared basalts/SWCNT composites. SEM indicated that the particle size of the nanosized basalt was 67.86 nm, in addition to the distribution of SWCNT in the basalt's matrix. At the same time, FTIR and Raman spectroscopies manifested the chemical functional groups in the nanosized basalts, namely, Si–O and (Si–O-Si) of SiO_4 of the jadeite, Fe–O of the magnetite, and TiO_6 octahedra of the ilmenite, besides the RBM, D, G, M +, G′, and 2G bands in the SWCNT. As expected, the pure nanosized basalts showed low electrical conductivity values, dielectric constant, and dielectric loss. In contrast, the nanosized basalts/SWCNT composites at SWCNT ratios 1, 3, and 5 wt% showed outstandingly increased electrical conductivity and dielectric constant; they showed thousands of folds compared with the pure nanosized basalts. Moreover, the theoretical calculations showed their excellent EMI shielding performance. The finding of this study is the possibility of preparing basalts/SWCNT composites and using them for practical applications in electrical devices, producing high conductive basalt fibers, and using them as materials for EMI shielding.

Declarations

Conflict of interest The authors declare that they have no conflict of interest.

Fig. 16 SEA, SER, and SET for a 2 mm thickness of the basalts/SWCNT nanocomposites versus SWCNT content at 10 GHz

References

1. M. Kiliç, Y. Karabul, M. Okutan, O. İçelli, J. Phys. Conf. Ser. **707**, 012054 (2016)

2. M. Anda, J. Shamshuddin, C.I. Fauziah, CATENA **124**, 147–161 (2015)
3. M. Çınar, M. Kılıç, Y. Karabul, N.Y. Canli, Ü. Alkan, M. Okutan, O. Içelli, J. Nanoelectron. Optoelectron. **11**, 477–483 (2016)
4. Y. Karabul, L. Amon Susam, O. İçcelli, Ö. Eyecioğlu, Nucl. Instrum. Methods Phys. Res. A. **797**, 29–36 (2015)
5. T. Deák, T. Czigány, Text Res. J. **79**, 645–651 (2009)
6. L.F. de Lima, J.E. Zorzi, R.C.D. Cruz, Boletín de la Sociedad Española de Cerámica y Vidrio **61**, 2–12 (2022)
7. P.A. Sabine, *In Encyclopedia of Planetary Science* (Springer, Netherlands, 1997), pp. 317–319
8. M. Pavlović, M. Dojčinović, R. Prokić-Cvetković, L. Andrić, Sci. Sinter. **51**, 409–419 (2019)
9. Z. Li, J. Ma, H. Ma, X. Xu, IOP Conf. Ser. Earth Environ. Sci. **186**, 012052 (2018)
10. C. Chang, X. Yue, B. Hao, D. Xing, P.-C. Ma, Carbon **167**, 31–39 (2020)
11. D.K. Rajak, D.D. Pagar, P.L. Menezes, E. Linul, Polymers **11**, 1667 (2019)
12. T. Bhat, V. Chevali, X. Liu, S. Feih, A.P. Mouritz, Compos. Part A **71**, 107–115 (2015)
13. K. Karvanis, S. Rusnáková, O. Krejčí, M. Žaludek, Polymers **12**, E1785 (2020)
14. H. Jamshaid, R. Mishra, V. Tunakova, J. Militky, Text Res. J. **87**, 715–725 (2016)
15. Z. Chen, T. Yu, Y.-H. Kim, Z. Yang, Y. Li, T. Yu, Compos. Sci. Technol. **203**, 108612 (2021)
16. N. Shentu, Hi-tech Fiber Appl. **30**, 7–13 (2005)
17. M.A. Ramazanov, H.A. Shirinova, F.V. Hajiyeva, D. Bychanok, J. Inorg. Organomet. Polym. Mater. **30**, 4783–4791 (2020)
18. A.M. Díez-Pascual, M. Naffakh, J.M. González-Domínguez, A. Ansón, Y. Martínez-Rubi, M.T. Martínez, B. Simard, M.A. Gómez, Carbon **48**, 3500–3511 (2010)
19. L. Liang, X. Wang, M. Wang, Z. Liu, G. Chen, G. Sun, Compos. Commun. **25**, 100701 (2021)
20. M. Burkov, A. Eremin, J. Mater. Eng. Perform **27**, 5984–5991 (2018)
21. J.A. Puértolas, J.F. García-García, F.J. Pascual, J.M. González-Domínguez, M.T. Martínez, A. Ansón-Casaos, Compos. Sci. Technol. **152**, 263–274 (2017)
22. K.J.D. MacKenzie, M.J. Bolton, J. Mater. Sci. **44**, 2851–2857 (2009)
23. Ü. Alkan, Y. Karabul, A.E. Bulgurcuoğlu, M. Kılıç, Z.G. Özdemir, O. İçelli, E-Polymers **17**, 417–425 (2017)
24. A. Saeed, S. Alomairy, C. Sriwunkum, M.S. Al-Buriahi, Radiat. Phys. Chem. **184**, 109454 (2021)
25. A. Saeed, S.O. Adewuyi, H.A.M. Ahmed, S.R. Al harbi, S.E. AlGarni, F. Abolaban, Silicon **14**, 5265–5276 (2021)
26. N. Baghdadi, A. Saeed, A.R. Ansari, A.H. Hammad, A. Afify, N. Salah, J. Alloys Compd. **869**, 159370 (2021)
27. S. Alraddadi, A. Saeed, H. Assaedi, J. Mater. Sci. Mater. Electron **31**, 11688–11699 (2020)
28. A. Saeed, M.S. Al-Buriahi, M.A.N. Razvi, N. Salah, F.E. Al-Hazmi, J. Mater. Sci. Mater. Electron **32**, 2075–2087 (2021)
29. N. Salah, N. Baghdadi, A. Alshahrie, A. Saeed, A.R. Ansari, A. Memic, K. Koumoto, J. Eur. Ceram. Soc. **39**, 3307–3314 (2019)
30. S.R. Alharbi, M. Alhassan, O. Jalled, S. Wageh, A. Saeed, J. Mater. Sci. **53**, 11584–11594 (2018)
31. O. Jalled, Z. Alharbi, S.R. Alharbi, A. Saeed, M. Alhassan, S. Al-Heniti, H.Y. Mohammed, Y. Al-Hadeethi, F. Al-Marzouki, A. Al-Mujtaba, J. Nanosci. Nanotechnol. **17**, 594–600 (2017)
32. G.A. Khater, M.M. Gomaa, J. Kang, Y. Yue, M.A. Mahmoud, Silicon **12**, 645–653 (2020)
33. M.S. Al-Buriahi, S. Alomairy, A. Saeed, A.S. Abouhaswa, Y.S. Rammah, Ceram. Int. **47**, 13065–13070 (2021)
34. A. Saeed, S.O. Adewuyi, H.A.M. Ahmed, S.R. Alharbi, S.E. Al Garni, F. Abolaban, Silicon **14**, 5265–5276 (2022)
35. R.M. Simon, Polym. Plast. Technol. Eng. **17**, 1–10 (1981)
36. Z. Li, Z. Wang, W. Lu, B. Hou, Metals **8**, 1026 (2018)
37. F. da Silvabruckmann, A.R. Viana, L.Q.S. Lopes, R.C.V. Santos, E.I. Muller, S.R. Mortari, C.R.B. Rhoden, J. Inorg. Organomet. Polym. Mater. **32**, 149–142 (2022)
38. C.M. Navarathna, N.B. Dewage, A.G. Karunanayake, E.L. Farmer, F. Perez, E.B. Hassan, T.E. Mlsna, C.U. Pittman, J. Inorg. Organomet. Polym. Mater. **30**, 214–229 (2020)
39. R. Jaiswal, K.V.S. Ranganath, J. Inorg. Organomet. Polym. Mater. **31**, 4504–4511 (2021)
40. H. Dai, H. Li, Z. Li, J. Zhao, X. Yu, J. Sun, Q. An, Sci. Rep. **9**, 2114 (2019)
41. F. Gendron, D. Smith, Ac. GendronBadou, J. Archaeol. Sci. **29**, 837–851 (2002)
42. A. Saeed, F. Abolaban, Biochem. Biophys. Res. Commun. **533**, 1048–1053 (2020)
43. A. Wang, K.E. Kuebler, B.L. Jolliff, L.A. Haskin, Am. Mineral **89**, 665–680 (2004)
44. O.N. Shebanova, P. Lazor, J. Solid State Chem. **174**, 424–430 (2003)
45. D.C. Smith, F. Gendron, J. Raman Spectrosc. **28**, 731–738 (1997)
46. Y. Park, K.P.S.S. Hembram, R. Yoo, B. Jang, W. Lee, S.-G. Lee, J.-G. Kim, Y.-I. Kim, D.J. Moon, J.-K. Lee, J.-K. Lee, J. Phys. Chem. C **123**, 14003–14009 (2019)
47. M.S. Dresselhaus, G. Dresselhaus, R. Saito, A. Jorio, Phys. Rep. **409**, 47–99 (2005)
48. T.L. Tan, L.L. Ng, L.C. Lim, Cosmos **09**, 47–56 (2013)
49. A.M.F. Lima, A.W. Musumeci, H.-W. Liu, E.R. Waclawik, G.G. Silva, J Therm. Anal. Calorim. **97**, 257 (2009)
50. M.A. Gabal, N.G. Al-Zahrani, Y.M. Al Angari, A.A. Al-Juaid, M.A. Abdel Fadeel, S.R. Alharbi, R.M. El-Shishtawy, Mater. Res. Express **6**, 105059 (2019)
51. Y. Wang and GJ. Weng, In: Micromechanics and Nanomechanics of Composite Solids. Electrical Conductivity of Carbon Nanotube- and Graphene-Based Nanocomposites, ed by SA. Meguid and GJ. Weng. (Springer, Cham) pp. 123–156 (2018)
52. M.A. Gabal, N.H. Al-Zahrani, Y.M.A. Angari, A. Saaed, IEEE Trans. Magn. **54**, 1–12 (2018)
53. M.A. Gabal, D.F. Katowah, M.A. Hussein, A.A. Al-Juaid, A. Awad, A.M. Abdel-Daiem, A. Saeed, M.M. Hessien, A.M. Asiri, ACS Omega **6**, 22180–22187 (2021)
54. M.A. Gabal, E.A. Al-Harthy, Y.M. Al Angari, A. Awad, A.A. Al-Juaid, A.M. Abdel Daiem, A. Saeed, J. Sol. Gel. Sci. Technol. **100**, 526–537 (2021)
55. K. Shimakawa, J. Phys. Colloques **42**, C164-170 (1981)
56. M. Fox, Am. J. Phys. **70**, 1269–1270 (2002)
57. M.A. Gabal, E.A. Al-Harthy, Y.M. Al Angari, A. Awad, A.A. Al-Juaid, M.A. Hussein, A.M. Abdel-Daiem, T.R. Sobahi, A. Saeed, J. Inorg Organomet. Polym. Mater. **32**, 1975–1987 (2022)
58. A.R. Tameev, L.L. Jiménez, L.Y. Pereshivko, R.W. Rychwalski, A.V. Vannikov, J. Phys. Conf. Ser. **61**, 1152–1156 (2007)
59. M.A. Gabal, W.A. Bayoumy, A. Saeed, Y.M. Al Angari, J. Mol. Struct. **1097**, 45–51 (2015)
60. S.A. Chernyak, A.S. Ivanov, N.E. Strokova, K.I. Maslakov, S.V. Savilov, V.V. Lunin, J. Phys. Chem. C. **120**, 17465–17474 (2016)
61. F. Bibi, C. Guillaume, N. Gontard, B. Sorli, Sens. Actuators B **250**, 76–84 (2017)
62. Q. Li, Q. Xue, L. Hao, X. Gao, Q. Zheng, Compos. Sci. Technol. **68**, 2290–2296 (2008)
63. K. Ahmad, W. Pan, S.-L. Shi, Appl. Phys. Lett. **89**, 133122 (2006)

64. M.A. Gabal, F. Al-Solami, Y.M. Al Angari, A. Awad, A.A. Al-Juaid, A. Saeed, Mater. Sci. Mater. Electron. **31**, 3146–3158 (2020)

65. M. Han, C.E. Shuck, R. Rakhmanov, D. Parchment, B. Anasori, C.M. Koo, G. Friedman, Y. Gogotsi, ACS Nano **14**, 5008–5016 (2020)

66. W. Jiang, F. Wu, Y. Jiang, M. Sun, K. Zhang, Y. Xia, D. Wang, A. Xie, Nanoscale **9**, 10961–10965 (2017)